Asian Journal of Chemistry; Vol. 30, No. 1 (2018), 183-190

ASIAN JOURNAL OF CHEMISTRY

https://doi.org/10.14233/ajchem.2018.20977

A Novel ^{18}F Labelled Imidazo-oxazolopyridine Derivative as β-Amyloid Imaging Agent: Synthesis and Preliminary Evaluation

SHIVANI SINGH[1,2], SWETA SINGH[1,*], ANJANI KUMAR TIWARI[1], RAKESH KUMAR SHARMA[2], RASHI MATHUR[1] and ANKUR KAUL[1]

[1]Division of Cyclotron and Radiopharmaceutical Sciences, Institute of Nuclear Medicine and Allied Sciences, Defence Research and Development Organisation, Brig. S.K. Mazumdar Road, Delhi-110 054, India
[2]Department of Chemistry, University of Delhi, Delhi-110 007, India

*Corresponding author: E-mail: swetadcrs2017@gmail.com

Received: 16 August 2017; *Accepted*: 29 September 2017; *Published online*: 30 November 2017; AJC-18673

Visualization of β-amyloid plaques in brain is pivotal for the diagnosis of Alzheimer's disease. In the present study, we have designed, synthesized and evaluated an imidazo-oxazolopyridine derivative, 2-[2-(4-fluorophenyl)imidazo[1,2-a]pyridine-6- yl]oxazolo[4,5-b]pyridine (FPIPOP) as a promising candidate for imaging of Aβ42 plaques using positron emission tomography (PET). Molecular docking of FPIPOP with Aβ42 fibrils predicted good affinity. The target compound was synthesized with high chemical yield and easily reproducible steps. In assays using thioflavin S as a competitive ligand, FPIPOP showed good affinity towards Aβ42 aggregates (K_i = 27.18 ± 4.7 nM). In PET experiments with normal Sprague dawley rat, high brain uptake and rapid clearance of activity was observed in cerebral cortex post i.v. injection (2.6 % ID/g for [^{18}F]FPIPOP at 1 min and 0.8 % ID/g at 60 min). [^{18}F]FPIPOP was found 76.4 % intact in brain for 60 min post injection. The ratio of radioactivity at maximal uptake to that at 60 min reached 20.5 for striatum, 26.4 for hippocampus and 33.1 for cerebellum. These results demonstrate that FPIPOP derivative has favourable *in vivo* brain pharmacokinetics and affinity for β-amyloid plaques; however, further optimization is required before pre-clinical evaluation of such skeletons in transgenic (T_g) mice models.

Keywords: Alzheimer's disease, β-Amyloid, Imaging, Positron emission tomography, Imidazo-oxazolopyridine derivative.

INTRODUCTION

One of the most common age related neurodegenerative disorders, Alzheimer's disease (AD), is a very complex disease. Till date, no therapeutic agent is known that can reverse the complex Alzheimer's disease symptoms. Thus, it is imperative to diagnose the disease at an early stage for timely intervention in disease advancement. Clinical diagnosis of Alzheimer's disease is based on indirect assessment of cognitive decline and mental disorder and does not recognise early neuropathological process. Neuropathologically, Alzheimer's disease can be characterized by the presence of neuropil threads, specific neuron loss and synaptic loss [1,2]. Detailed mechanism of Alzheimer's disease pathology is still elusive, however, the most common hallmarks of Alzheimer's disease including extracellular deposition of senile plaques composed of β-amyloid and intracellular neurofibrillary tangles composed of hyperphosphorylated tau protein are considered to be important causative events in Alzheimer's disease pathologies [3]. Also, as per the amyloid cascade hypothesis, senile plaques are considered as a major pathological characteristic of Alzheimer's disease [4]. Thus, a comprehensive analysis of both the hallmarks needs to be carried out for an accurate diagnosis of Alzheimer's disease. Some of the leads to identify Aβ probes through positron emission tomography (PET) includes C-11 and F-18 labelled PET tracers for clinical applications like (N-[^{11}C]-methyl)-6-OH-BTA-1, Pittsburg compound B ([^{11}C]PiB) [5,6] and its F-18 derivative 3'-[^{18}F]FPiB (Flutemetamol, GE-067) [7,8], [^{11}C]SB-13 [9], [^{18}F]Florbetaben (BAY-949172) [10], [^{18}F]Florbetapir (AV-45) [11,12] and [^{18}F]FDDNP [13] (Fig. 1). Most of the above mentioned imaging agents are derivatives of stilbene and thioflavin T. Due to their planar geometry, they get easily fit into the hydrophobic grooves of the aggregated Aβ plaques. C-11 labelled tracers are found to be effective preclinically towards Aβ plaques, but the short half-life of C-11 (~ 20.3) limits its use as a radio-isotope for labelling the agents at PET imaging centres without cyclotron facility [14]. The longer half-life of the F-18 (~109.7 min) makes it a radioisotope of choice in the area of diagnostic imaging and can be used at PET imaging sites farther away from radio-nuclide production sites, making them easily accessible for patients.

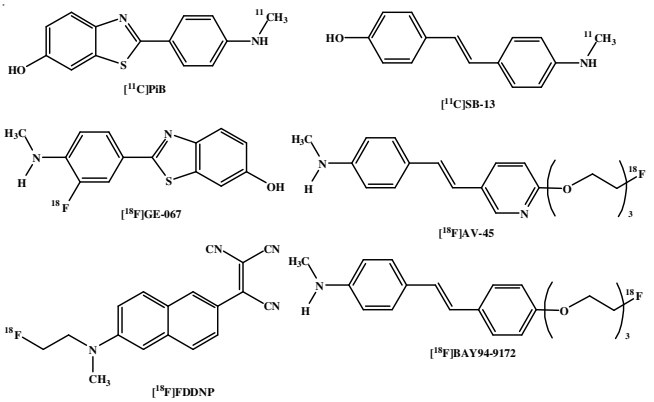

Fig. 1. Chemical structures of representative C-11 and F-18 Aβ plaques imaging agents

Also, currently available F-18 labelled compounds are disadvantaged by a higher unspecific binding, *i.e.* to white matter, as compared to their C-11 labelled analogues. Thus, despite the high load of Aβ in advanced Alzheimer's disease cases, the tracer uptake ratios Alzheimer's disease patients/ healthy controls of [^{18}F]FDDNP and [^{18}F]Florbetaben in brain regions known to contain Aβ have been found to be 1.3 [15] and 1.5 [16], respectively. Thus, a new F-18 radiopharmaceuticals with improved pharmacokinetics are required for advances in this field.

A successful amyloid imaging agent must be specific for Aβ with minimal nonspecific binding in order to provide a large specific signal for plaque detection [14-19]. The primary aspect of *in vivo* brain imaging is to check BBB permeability, brain uptake profile and release kinetics from regional brain sections. Previous reports on β-amyloid imaging agents confirmed that highly lipophilic tracers display high uptake and longer retention in white matter, which can affect the signal-to-noise ratio in imaging studies and make it difficult to differentiate between Alzheimer's disease and non-Alzheimer's disease patients [14]. Therefore, optimal lipophilicity (*e.g.*, c log P) is one criterion that must be employed to decrease non-specific binding to brain tissues [11]. Recently, ^{18}F-benzoxazolopyridine, MK-3328 [20] has been reported as candidate probes for the imaging of senile plaques in Alzheimer's disease brains. It showed comparable results with IMPY (6-iodo-2-(4'-dimethylamino)phenyl-imidazo[1,2-*a*]pyridine) [21-24] in terms of uptake in small animal models. In this work, we have used MK-3328 and IMPY scaffolds for synthesizing an imidazo-oxazolopyridine based derivative 2-[2-(4-fluorophenyl)imidazo[1,2-a]pyridine-6-yl]-oxazolo[4,5-b]pyridine (FPIPOP), radio-labelled with F-18 and evaluated its efficacy as a PET tracer for β-amyloid imaging. The binding of FPIPOP with Aβ42 has been confirmed by *in silico* and *in vitro* competitive studies.

EXPERIMENTAL

The solvents and reagents consumed were purchased from commercial sources and used without any further purification. Purification of the synthesized compounds using column chromatography was carried using silica MN60 (60-120) and TLC sheets coated with silica gel 60, F_{254} (Merck). The characterization using ^{1}H and ^{13}C NMR was done on Bruker Avance II 400 MHz. chemical shifts are reported with respect to TMS. HPLC analysis were performed using a JASCO HPLC system. The monitoring of effluent radioactivity was done using a NaI (Tl) scintillation detector system.

Synthesis of 5-(oxazolo[4,5-b]pyridine-2-yl)pyridine-2-amine (1): A mixture of 2-amino-3-hydropyridine (0.5 g, 4.5 mmol), 6-aminonicotinic acid (0.62 g, 4.5 mmol) and polyphosphoric acid (10 g) was heated to 220 °C for 4 h. the reaction mixture was cooled to room temperature and poured into 10 % potassium carbonate solution (~ 400 mL). The precipitate was collected by filtration under reduced pressure to give 0.70 g (73 %) of the product. Recrystallization of the product in methanol gave the pure product. δ_H (400 MHz; DMSO; Me_4Si): 8.78 (1H, d. *J* = 2.0 Hz, CH), 8.44 (1H, dd, *J* = 1.6, 4.8 Hz, CH), 8.11 (1H, d, *J* = 1.6 Hz, CH), 8.09 (1H, t, *J* = 1.2 Hz, CH), 7.33 (1H, dd, *J* = 5.2, 8.0 Hz, CH), 7.00 (2H, s, NH_2), 6.61 (1H, d, *J* = 8.8 Hz); δ_C (100 MHz; DMSO; Me_4Si): 165.28 (C), 162.66 (CH), 156.43 (C), 149.65 (CH), 146.33 (C), 142.66 (CH), 136.43 (CH), 120.12 (C), 118.61 (CH), 110.27 (C), 108.50 (CH); ESI-MS(+): *m/z* [M+H$^+$] calcd. (found): 213 (213).

Synthesis of 2-bromo-1-(4-nitrophenyl)ethanone (2): 1-(4-Nitropheny)ethanone (1.0 g, 6.05 mmol) and tetra-*n*-butylammonium tribromide (3.82 g, 7.96 mmol) were taken in methanol (100 mL). The reaction was stirred at room temperature overnight. The solvent was then removed under reduced pressure and the residue was dissolved in AcOEt (60 mL). The mixture was washed twice with water (2 × mL) and once with brine. The organic solution was then dried over Na_2SO_4 and the solvent from the filtrate was removed. The crude product was purified using FCC (hexane-CH_2Cl_2) (1:1 v/v + 2 % AcOEt), yielding the desired product as a yellow solid (0.970 g, 4.47 mmol, 62 %). δ_H (400 MHz; DMSO; Me_4Si): δ 8.34 (2H, d, *J* = 8.8 Hz, CH), 8.21 (2H, d, *J* = 8.8 Hz, CH), 5.01 (2H, s, CH_2Br). δ_C (100 MHz; DMSO; Me_4Si): 191.40 (-CO-), 150.61 (C), 139.13 (C), 130.60 (C), 124.38 (C), 34.79 (-CH_2Br-).

Synthesis of 2-[2-(4-nitrophenyl)imidazo[1,2-α]-pyridine-6-yl]oxazolo[4,5-b]pyridine (3): Compound **1** (0.5 g, 2.35 mmol) and compound **2** (0.690 g, 2.83 mmol) were taken in absolute ethanol (65 mL) and stirred under reflux for 2 h. the mixture was then cooled and $NaHCO_3$ (0.237 g, 2.83 mmol) was added. The reaction mixture was refluxed for another 4 h. the resultant precipitate was filtered and the solid product was washed with DCM and EtOH, yielding the title compound as an orange solid (0.490 g, 63 % yield). δ_H (400 MHz; DMSO; Me_4Si): 9.66 (1H, s, CH), 8.85 (1H, s, CH), 8.59 (1H, s, CH), 8.35 (2H, d, *J* = 8.7 Hz, CH), 8.30 (1H, d, *J* = 8.7 Hz, CH), 7.95 (1H, d, *J* = 5.2 Hz, CH), 7.89 (1H, s, CH), 7.79 (1H, d, *J* = 5.2 Hz, CH), 7.45 (2H, s, CH); ESI-MS(+): *m/z* [M$^+$] calc (found): 357 (357).

Synthesis of 2-[2-(4-fluorophenyl)imidazo[1,2-α]-pyridine-6-yl]oxazolo[4,5-b]pyridine (4): Compound **3** (0.1 g, 0.28 mmol) and cesium fluoride (0.212 g, 1.4 mmol) was added in dry DMSO (10 mL) under N_2. The reaction mixture was heated at 120 °C for 1.5 h. TLC (9:1 DCM/MeOH) showed complete conversion of the nitro compound to fluoro substituted product. Then, distilled water is added to the reaction mixture and extraction with EtOAc (3 × 20 mL) and concentrated *in vacuo*. The crude product was purified using column

chromatography (DCM/MeOH) yielding 0.084 g (92 %) of an orange product. δ_H (400 MHz; DMSO; Me_4Si): 9.53 (1H, s, CH), 8.53 (1H, s, CH), 8.50 (1H, d, *J* = 4.4 Hz, CH), 8.20 (1H, d, *J* = 8.4 Hz, CH), 7.97 (1H, q, *J* = 1.6 Hz, CH), 7.91 (2H, d, *J* = 8.4 Hz, CH), 7.74 (1H, d, *J* = 10 Hz, CH), 7.42 (1H, *J* = 3.2 Hz, 1H), 7.19 (2H, d, *J* = 8.4 Hz, CH); δ_C (100 MHz; DMSO; Me_4Si): 163.75 (CH), 130.62 (2CH), 129.06 (CH), 128.33 (C), 128.25 (C), 123.37 (CH), 121.33 (CH), 120.37 (2CH), 119.48 (CH), 117.62 (CH); ESI-MS(+): *m/z* [M+H$^+$] calc (found): 331 (331).

Radiosynthesis of 2-[2-(4-^{18}F-fluorophenyl)imidazo[1,2-α]pyridine-6-yl]oxazolo[4,5-b]pyridine ([^{18}F]FPIPOP) [^{18}F]4: [^{18}O]H_2O (95 %) was used for ^{18}F production. [^{18}F]HF was extracted and separated from the cyclotron target by elution with [^{18}O]H_2O, respectively. H[^{18}F]F was concentrated on a short QMA column followed by elution with 400 µL of a solution with aqueous K_2CO_3 (10 mg/8 mL), Kryptofix®222 (30 mg) in MeCN (8 mL). Aqueous K[^{18}F]F was transferred to a reaction vial and evaporated to remove H_2O and MeCN at 110 °C for 15 min. after 3 (2 mg) in 1,2-dichlorobenzene (150 µL) was added to the vial, the reaction gas (10 mL min^{-1}) for 2 min and trapped in a solution of DMSO (300 µL). After the radioactivity plateaued, the reaction mixture was heated at 120 °C for 15 min. HPLC purification was carried out using a mobile phase of MeCN-H_2O-Et_3N (6.0/4.0/0.01, v/v/v) and flow rate was maintained at 5.0 mL min^{-1}. Desired radiolabelled product was collected in a sterile flask followed by evaporated to dryness *in vacuo*. Further, redissolved in 3 mL of sterile normal saline and passed through a 0.22 µm Millipore filter. The retention time of [^{18}F]FPIPOP] was 9.7 min for purification and 9.6 min for analysis on HPLC [30].

Determination of lipophilicity: The experimental determination of partition coefficients of [^{18}F]FPIPOP and was performed in 1-octanol and 0.02 M phosphate buffer at a pH of 7.4. Both the phases were pre-saturated with each other. 1-Octanol (3 mL) and phosphate buffer (3 mL) were taken into a test tube containing 0.38 MBq of [^{18}F]FPIPOP. The test tube was vortexed for 10 s and centrifuged (5 min, 4000 rpm). Aliquots of 500 µL from the 1-octanol and buffer phases were transferred into a new test tube. 1-Octanol (2 mL) and phosphate buffer (3 mL) were taken into the same test tube. The centrifuging, vortexing and counting were repeated. The amount of radioactivity was measured in each tube with a γ counter and corrected for decay. The partition coefficient was calculated using eqn. 1: (counts/µL in 1-octanol)/(counts/µL in buffer) = r.

All assays were performed in triplicate.

***Ex vivo* biodistribution study:** Biodistribution study was carried out in the SD rat. [^{18}F]FPIPOP (1.85 MBq, 10 pmol) was injected through the tail vein and animals were sacrificed at six time intervals (2, 5, 15, 30 and 60 min). Blood samples were collected at each time point from each group (n = 4) and the adrenal gland, brain, heart, kidneys, liver, lungs, spleen, small intestine and testis were quickly removed and weighed. Radioactivity counts in each tissue/organ, at each time point was done by a 1480 Wizard 3" autogamma counter (Perkin Elmer, Waltham, MA, USA). It is expressed as the percentage of the injected dose per gram of the wet tissue (% ID/g). The decay correction was taken into consideration during the radioactivity counts.

Radiometabolite analysis: The SD rats were intravenously injected with [^{18}F]FPIPOP (7.5 MBq per rat) through the tail vein. The animals were sacrificed by cardiac puncture at 5, 15, 30 and 60 min (n = 3 for each point). Blood (0.8-1.0 mL) and the entire brain samples were obtained and treated as reported previously. The supernatant of the brain homogenate and plasma was analyzed under the following conditions: Capcell Pack UG80 C18 column, 4.6 mm i.d. × 250 mm; MeCN-H_2O-Et_3N, 6/4/0.01(v/v/v); flow rate, 1.0 mL/min. the percentages of the intact [^{18}F]FPIPOP were calculated, simultaneously, the radioactivity fractions in the HPLC waste solution were measured using a 1480 Wizard 3" auto-gamma counter.

PET study and image analysis: A small-animal PET scanner from Siemens Medical Solutions was used for imaging. Normal SD rats were anaesthetized during the scan and the animals' body temperature was maintained at 40 °C using water circulation system (T/Pump TP401, Gaymar Industries). The emission scans were acquired at different time intervals post injection of [^{18}F]FPIPOP (5.18 ± 0.29 MBq/0.02-0.04 nmol) through the tail vein. All image frames were summed at 0-30 min. The time activity curves (TACs) for the striatum, hippocampus and cerebellum were generated from the PET data in order to parameterize the radioactivity uptake, clearance and distribution in healthy rat. The radioactivity (% ID/g) was estimated as the ratio of the regional activity concentration normalized by the injected dose {SUV = [(MBq/g of tissue)/(MBq injected/patient body in g)]} and the weight of the animal to give the PET-generated biodistribution pattern over different parts of brain.

***In vitro* binding assay with Aβ42 and tau aggregates:** The K_i and K_d values of [^{18}F]FPIPOP binding to the tau aggregates and synthetic Aβ42 aggregates purchased from Sigma Aldrich were determined utilizing methods previously reported [31]. The values of K_d and B_{max} were determined using GraphPad Prism 7 XML software.

Animals: Sprague-Dawley (SD) rats (male, 8-9 weeks old, 240-330 g) were taken for studies. Animals were kept under optimal conditions with a 12/12 h dark/light cycle and animals were handled as per recommendations of ethical committee.

RESULTS AND DISCUSSION

Computational analysis of FPIPOP: In order to design and synthesize Aβ plaques imaging agent with optimum lipophilicity, good binding affinity and higher specificity, we began with docking study (Schrödinger Maestro 9.4) of newly designed ligand with the 3D structure of Aβ42 was obtained from protein data bank (PDB: 2BEG) [25]. After the optimization of model, as the exact binding site was unknown, we zeroed in on three major binding sites (Fig. 2). Two of them were within the fibril whereas one was on the surface of the two sites of Met35. Site 1 is constituted by terminal residues (Leu17, Val18, Phe19, Gly38 and Val40) and is in the proximity of the solution environment, which is favourable for ligand access in this peptide. At this site, the ligand showed hydrophobic interactions. Solvent interactions are also exhibited by the backbone of FPIPOP. Site 2 is deeply buried inside the fibril and thus has a highly hydrophobic environment. It is constituted by side chains of Phe19, Ala21 and Val36 and the backbone atoms of Phe20

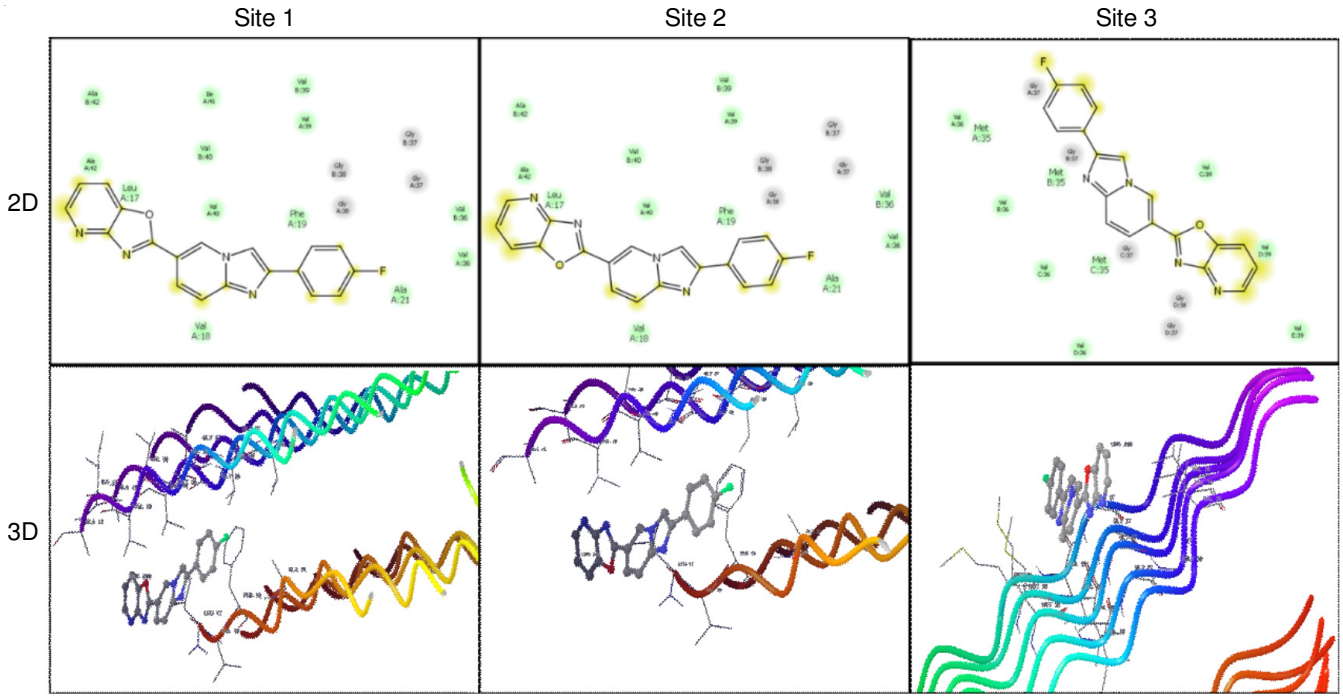

Fig. 2. 2D/3D interactions of FPIPOP with Aβ42 (PDB: 2BEG)

and Gly37. In this site, the ligand interacted hydrophobically besides solvent interactions. Site 3 is exposed to solution. These results encouraged us to synthesize the oxazolopyridine derivative for imaging of Aβ42 plaque with high specificity.

All the interactions of the ligand with protein at the three sites with their glide scores are given in Table-1 (molecular docking interactions of ligand with protein and their docking scores). All these interactions and docking scores showed that there is a reversible binding of the ligand at the binding sites of protein and hydrophobic interactions are the dominant forces in binding.

Synthesis and characterization of tracer 2-[2-(4-fluorophenyl)imidazo[1,2-a]pyridine-6-yl]oxazolo[4,5-b]pyridine (FPIPOP): Thus a new ligand FPIPOP was prepared as outlined in **Scheme-I**. Firstly, 2-amino-3-hydroxypyridine was cyclized with 6-aminonicotinic acid into an oxazolopyridine using polyphosphoric acid to give **1** having yield of 73 %. 4-Nitroacetophenone was brominated using TBATBr (tetrabutylammonium tribromide) with 62 % yield to give 4-nitrophenacylbromide (**2**). Further, we carried out condensation of **1** with 4-nitrophenacylbromide (**2**) to give **3** with 63 % yield. Finally, to get the target compound 2-[2-(4-fluorophenyl)imidazo[1,2-a]pyridine-6-yl]oxazolo[4,5-b]pyridine (FPIPOP), the compound **3** was fluorinated using cesium fluoride to give compound **4** with 92 % yield. It was successfully characterized by ^{1}H, ^{13}C NMR and mass spectrometry and the purity was established by HPLC (≥ 97 %) with a retention time of R_t = 9.6 min. The ^{18}F radiolabelling was performed with K[^{18}F]F-K_{222} by nucleophilic aromatic nitro-to-fluoro substitution in DMSO by heating at 120 °C for 15 min as shown in **Scheme-II**. The radiochemical yield of [^{18}F]FPIPOP was 29 ± 4 % (n = 5) and was based on [^{18}F]F^{-}, which was corrected for physical decay during the reaction times of 61 ± 5 min from the end of bombardment. The specific activity calculated to be in the range of 143 ± 12 GBq/μmol (n = 3) at EOS. The identity of [^{18}F]FPIPOP was verified by a comparison of retention time with the nonradioactive compound. To assess the potential of our synthesized agent for CNS directed application, lipophilicity was determined. The log P value of the synthesized compound was found to be 3.5 ± 0.34. This is within the optimum range of a suitable brain imaging agent.

***In vitro* binding studies:** It is necessary to evaluate the selectivity of FPIPOP for Aβ42 as both Aβ42 and tau aggregates possess β-sheeted structure. Thus, to evaluate the binding affinity of FPIPOP for both Aβ42 and tau aggregates, an assay using thioflavin S (ThS) as a competitive ligand was carried out (Fig. 3). K_i value of FPIPOP for Aβ42 was found out to be 27.18 ± 4.7 nM whereas for tau aggregates, it was found out to be 87.19 ± 3.9 nM (ratio of ~3). Clearly, FPIPOP exhibits higher selectivity for Aβ42 over tau aggregates.

TABLE-1
MOLECULAR DOCKING INTERACTIONS OF LIGAND WITH PROTEIN AND THEIR DOCKING SCORES

Binding site	Interacting residues	Docking score (kcal/mol)
Site 1	Leu (A:17), Val (A:18), Phe (A:19), Ala (A:21), Val (A:36), Val (B:36), Val (A:39), Val (B:39), Val (A: 40), Val (B:40), Ile (A:41), Ala (A:42) and Ala (B:42)	-4.426
Site 2	Leu (A:17), Val (A:18), Phe (A:19), Ala (A:21), Val (A:36), Val (B:36), Val (A:39), Val (B:39), Val (A:40), Val (B:40), Ala (A:42), Ala (B:42)	-4.924
Site 3	Met (A:35), Met (B:35), Met (C:35), Val (A:36), Val (B:36), Val (C:36), Val (D:36), Val (C:39), Val (D:39), Val (E:39)	-4.827

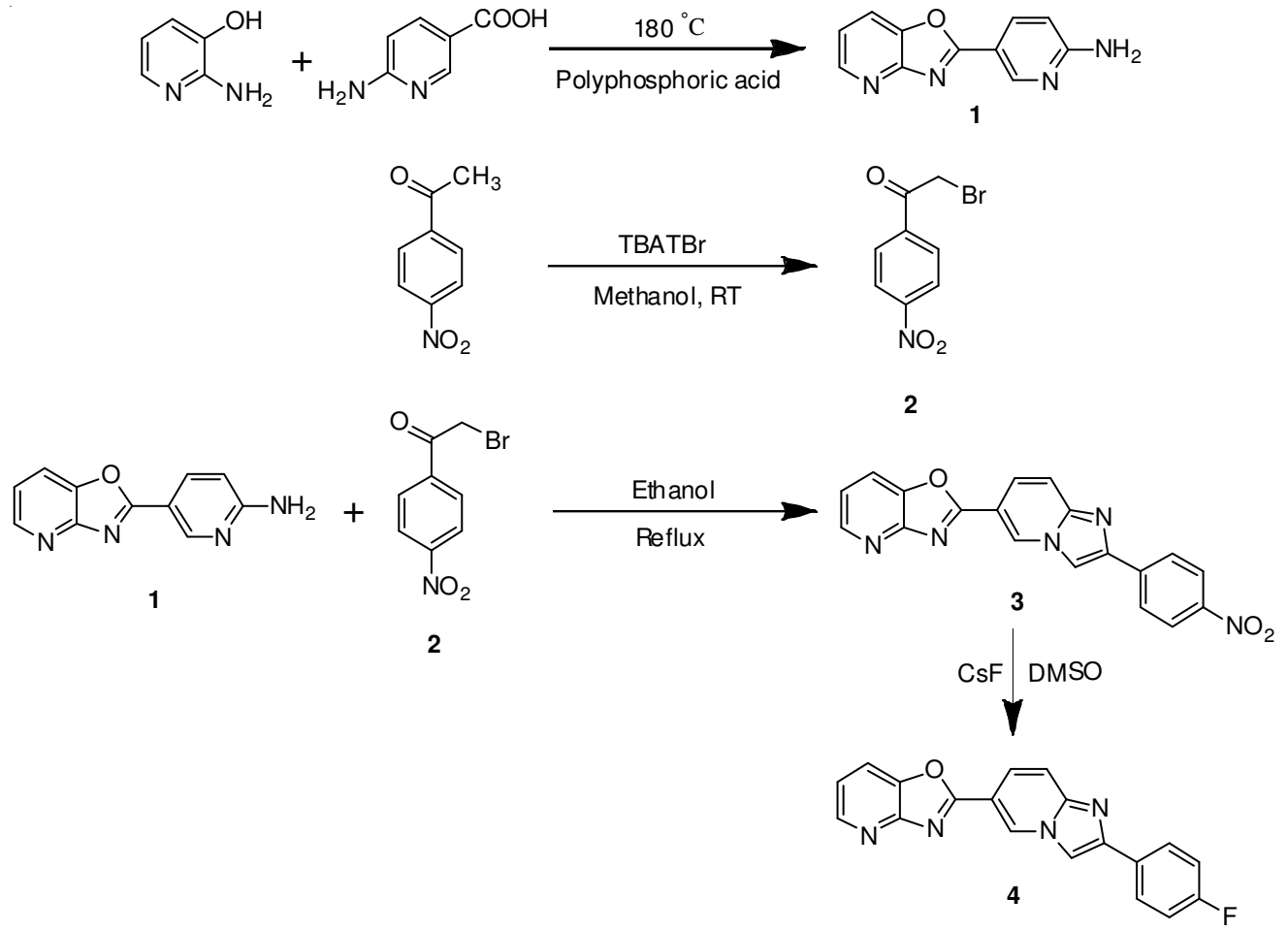

Scheme-I: Synthesis of 2-(2-(4-fluorophenyl)imidazo[1,2-a]pyridin-6-yl)oxazolo[4,5-b]pyridine (FPIPOP)

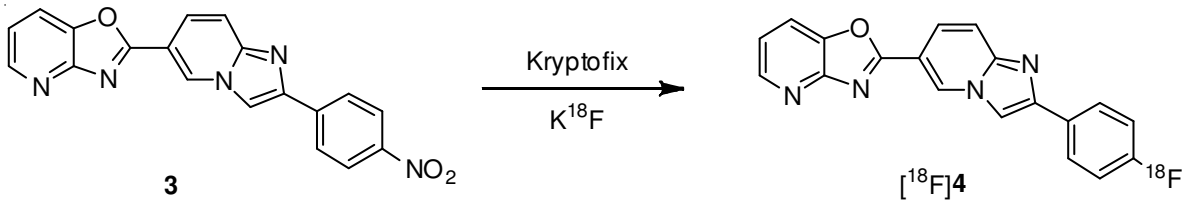

Scheme-II: Synthesis of 2-(2-(4-[^{18}F]fluorophenyl)imidazo[1,2-a]pyridin-6-yl)oxazolo[4,5-b]pyridine ([^{18}F]FPIPOP)

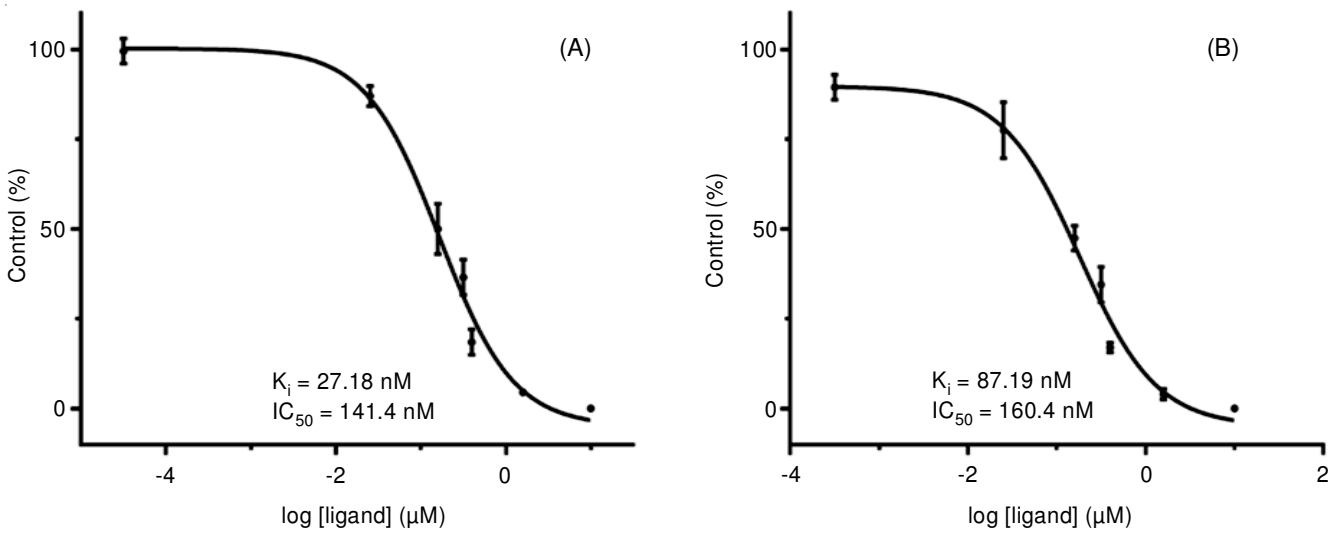

Fig. 3. Inhibition curves for binding of thioflavin S to Aβ42 (A) and tau (B) aggregates using FPIPOP as test compound (n = 3)

In competitive inhibition assays, FPIPOP competed with thioflavin S to bind to both Aβ42 and tau aggregates. To verify that FPIPOP binds directly to these aggregates, saturation binding assays of [^{18}F]FPIPOP to these aggregates were performed. A scatchard analysis demonstrated the K_d value and B_{max} of FPIPOP for both tau and Aβ42 aggregates (K_d = 238.2 nM and B_{max} = 438.4 pmol/nmol tau protein for tau aggregates and K_d = 47.6 nM and B_{max} = 99.72 pmol/nmol Aβ42 protein for Aβ42 aggregates). These results revealed that FPIPOP had selective affinity for Aβ42 over tau aggregates validating the K_i values of FPIPOP for both the aggregates in the competitive inhibition assays with thioflavin S as a competitive ligand.

***Ex vivo* biodistribution study:** Studies of biodistribution and metabolic profile of any radiopharmaceutical agent is pre-requisite for clinical translation. For evaluation of biological distribution of [^{18}F]FPIPOP, healthy SD rat models were used. In SD rat model, a compound with favourable characteristics for plaque imaging should not only have high affinity for β-amyloid but also show a high initial brain uptake followed by a rapid washout, indicating absence of non-specific binding to any brain tissue lacking β-amyloid. Thus, to assess the pharmacokinetics of our ligand, we performed *in vivo* biodistribution experiments with the [^{18}F]FPIPOP in healthy SD rats (n=3) without Aβ deposits in their brain at different time intervals post injection (Fig. 4). The percent injected activity (% IA) associated with each organ was determined based on the activity measured per gram of organ or tissue. [^{18}F]FPIPOP showed high uptake in brain. The observed activity was 2.6 ± 0.31 % ID/g in cerebral cortex and 2.65 ± 0.25 % ID/g in cerebellum at 2 min post injection, sufficient for acquiring PET image. This is comparable to the initial uptake of its parent compound ([^{125}I]IMPY, 2.88 ± 0.25 % ID/g at 2 min post-injection) [23]. A brain uptake of > 0.5 % ID/g at initial time period of 2 min post-injection is preferred for Aβ imaging tracers [26]. The tracer [^{18}F]FPIPOP exhibited ~4-fold higher uptake than the pre-requisite for a prospective Aβ imaging agent. At 60 min post injection, the uptake was 0.7 ± 0.06 % ID/g in cerebral cortex and 0.8 ± 0.26 % ID/g in cerebellum, indicating a relatively fast washout from the brain. [^{18}F]FPIPOP showed high initial uptake and rapid clearance from normal brain validating absence of Aβ plaques. [^{18}F]FPIPOP was cleared from plasma mainly by the renal route (15.6 % ID/g in the kidney at 15 min post-injection) and radioactivity was observed to accumulate within the intestine at later time points (2.8 % ID/g at 60 min post-injection). The radioactive signal elevated in lungs 1 min after tracer injection, then decreased at the 15 min time point. The transient high lung uptake reflects the large blood volume of this blood-rich organ [27].

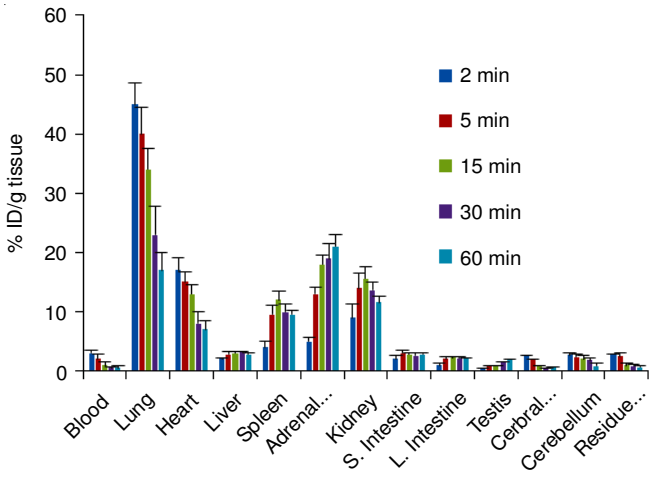

Fig. 4. Biodistributon of [^{18}F]FPIPOP after tracer injection in normal Sprague Dawley (SD) rat (n=3)

Radiometabolite analysis: Since PET can't discriminate between signals from parent radioligand metabolites and if both are present in brain, it is necessary that PET radioligands do not undergo rapid metabolism over the period of PET acquisition. Thus it is necessary to verify the formulation of metabolites to ensure PET signals of the intact parent compound. Characterization of radiometabolites of [^{18}F]FPIPOP in the rat brain and plasma was carried out for a period of over 60 min after bolus injection of [^{18}F]FPIPOP (Fig. 5). HPLC fractions of metabolite from rat brain homogenate were collected and analyzed by LC-MS. It was appreciably stable in brain with 75 % of the parent radioligand intact even at 60 min post injection in brain whereas it was rapidly metabolized in plasma with only 3.9 % intact tracer present at 60 min post injection. Only one polar metabolite emerged during 60 min studies and it was found to be able to cross the BBB. This small percentage of the metabolite should not interfere in the imaging of Aβ plaques provided the metabolite doesn't enter and bind in the compartment of interest.

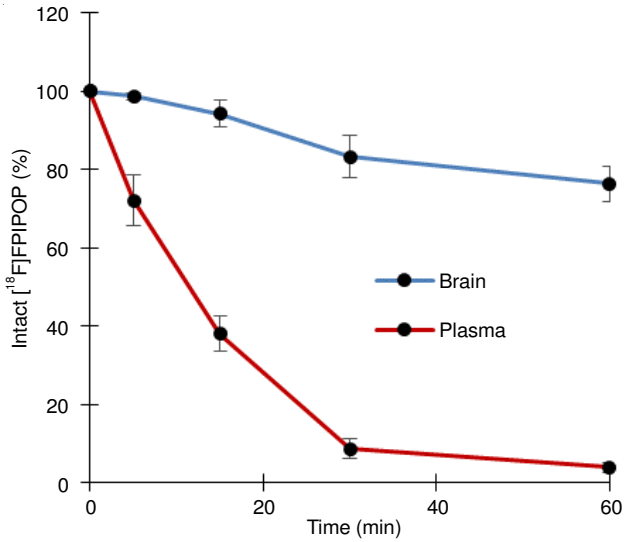

Fig. 5. Radiometabolite study of [^{18}F]FPIPOP in plasma and brain of SD rat

***In vivo* PET examination:** To further evaluate the uptake in brain, PET study in normal rat was performed. The PET images (summed 1-30 min post injection) of different brain sections (sagittal, coronal and transversal) were acquired (Fig. 6). PET images showed relatively low activity in all the sections, which indicates that [^{18}F]FPIPOP does not have prolonged retention in the normal brain. This finding further corroborates the pharmacokinetics results. Since no tracer uptake was observed in the skull, it was concluded that [^{18}F]FPIPOP does not show substantial defluorination *in vivo* [28].

PET Time activity curves: To further validate the pharmacokinetics of the present compound, time activity curves (TACs) of [^{18}F]FPIPOP for brain regions of a rat was also carried out (Fig. 7). The initial uptake of radioactivity into all brain regions

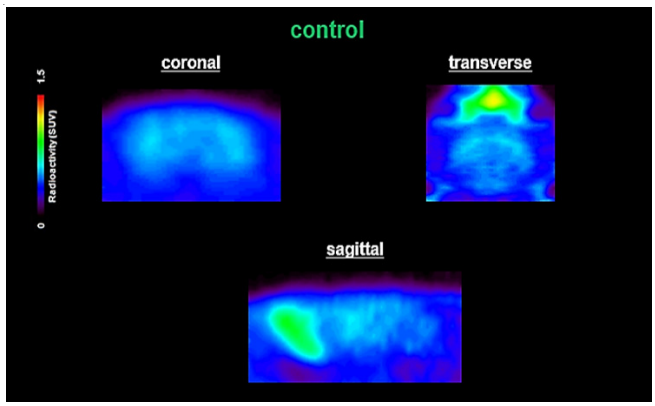

Fig. 6. PET images of [^{18}F]FPIPOP in normal SD rat brain summed at 0-30 min (sagittal, coronal and transversal)

was rapid and high. Striatum showed the highest uptake of radioactivity. The radioactivity washed out continuously from all brain regions and at a similar rate all over the duration of the scan. The uptake in the brain, as shown in time activity curves, remains in concordance with the biodistribution results. The ratio of the radioactivity at maximal uptake to that at 60 min reached 20.5 for striatum, 26.4 for hippocampus and 33.1 for cerebellum. For prospective high-affinity radioligands for imaging β-amyloid plaques with PET, the ratios of radioactivity in normal animal brains at maximal level and at a later specific time (*e.g.*, 60 min after injection) are considered to be predictive of the signal-to-noise ratio that might be achievable when β-amyloid plaques are present [29]. So, in this respect the ligand [^{18}F]FPIPOP showed superiority over [^{125}I]IMPY [23].

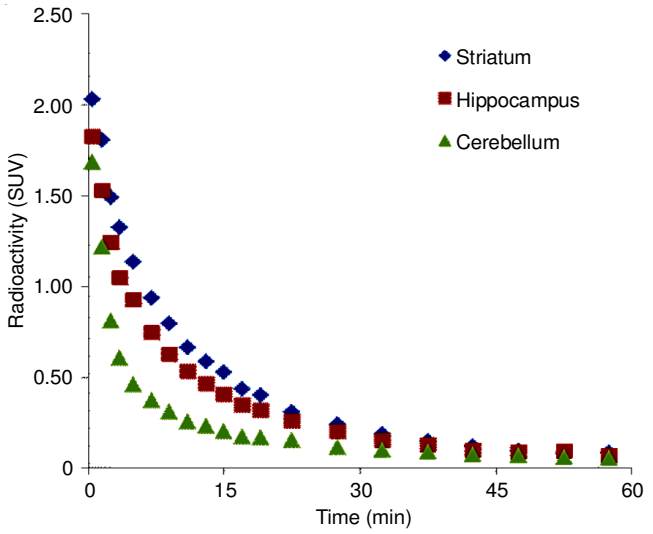

Fig. 7. Time activity curves of [^{18}F]FPIPOP in SD rat at different time intervals (0-60 min) expressed as radioactivity (SUV) *versus* time (min)

Conclusion

In conclusion, we have designed, synthesized and assessed a new fused skeleton imidazo[1,2-a]pyridine-6-yl)oxazolo[4,5-b]pyridine, [^{18}F]FPIPOP as a novel PET ligand for imaging of Aβ42 aggregates in Alzheimer's disease. *In vitro* binding assay demonstrated good selectivity of FPIPOP for Aβ42 over tau aggregates. However, FPIPOP displayed only moderate affinity towards Aβ42. *Ex vivo* biodistribution study showed good initial brain uptake and fast washout. Metabolite study of [^{18}F]FPIPOP did not show any significant defluorination. The ratio of radioactivity at maximal uptake to that at 60 min (predictive of the signal-to-noise ratio) was found out to be good. Further structural modification of current scaffold such as introducing the substituent and study of their position to improve the affinity for Aβ42 may lead to the development of better and more useful diagnostic agents. Further studies are also required to prove the efficacy in transgenic animal models along with a look into smaller to higher longitudinal animal studies to optimize the final skeleton before further use.

ACKNOWLEDGEMENTS

The authors express their gratitude to Dr. A.K. Singh, Director, Institute of Nuclear Medicine and Allied Sciences, Defence Research and Development Organization for his guidance and support. Thanks are also due to Council of Scientific and Industrial Research, Delhi, India for the award of senior research fellowship.

REFERENCES

1. V. Cavallucci, M. D'Amelio and F. Cecconi, *Mol. Neurobiol.*, **45**, 366 (2012); https://doi.org/10.1007/s12035-012-8251-3.
2. M.P. Murphy and H. LeVine III, *J. Alzheimers Dis.*, **19**, 311 (2010); https://doi.org/10.3233/JAD-2010-1221.
3. C.C. Rowe and V.L. Villemagne, *J. Nucl. Med. Technol.*, **41**, 11 (2013); https://doi.org/10.2967/jnumed.110.076315.
4. E. Karran, M. Mercken and B.D. Strooper, *Nat. Rev. Drug Discov.*, **10**, 698 (2011); https://doi.org/10.1038/nrd3505.
5. C.A. Mathis, Y. Wang, D.P. Holt, G.-F. Huang, M.L. Debnath and W.E. Klunk, *J. Med. Chem.*, **46**, 2740 (2003); https://doi.org/10.1021/jm030026b.
6. W.E. Klunk, H. Engler, A. Nordberg, Y. Wang, G. Blomqvist, D.P. Holt, M. Bergström, I. Savitcheva, G.F. Huang, S. Estrada, B. Ausen, M.L. Debnath, J. Barletta, J.C. Price, J. Sandell, B.J. Lopresti, A. Wall, P. Koivisto, G. Antoni, C.A. Mathis and B. Långström, *Ann. Neurol.*, **55**, 306 (2004); https://doi.org/10.1002/ana.20009.
7. M. Koole, D.M. Lewis, C. Buckley, N. Nelissen, M. Vandenbulcke, D.J. Brooks, R. Vandenberghe and K. Van Laere, *J. Nucl. Med.*, **50**, 818 (2009); https://doi.org/10.2967/jnumed.108.060756.
8. M. Romano and E. Buratti, *Drugs Today (BARC)*, **49**, 181 (2013).
9. M. Ono, A. Wilson, J. Nobrega, D. Westaway, P. Verhoeff, Z.P. Zhuang, M.P. Kung and H.F. Kung, *Nucl. Med. Biol.*, **30**, 565 (2003); https://doi.org/10.1016/S0969-8051(03)00049-0.
10. V.L. Villemagne, K. Ong, R.S. Mulligan, G. Holl, S. Pejoska, G. Jones, G. O'Keefe, U. Ackerman, H. Tochon-Danguy, J.G. Chan, C.B. Reininger, L. Fels, B. Putz, B. Rohde, C.L. Masters and C.C. Rowe, *J. Nucl. Med.*, **52**, 1210 (2011); https://doi.org/10.2967/jnumed.111.089730.
11. D.F. Wong, P.B. Rosenberg, Y. Zhou, A. Kumar, V. Raymont, H.T. Ravert, R.F. Dannals, A. Nandi, J.R. Brasic, W. Ye, J. Hilton, C. Lyketsos, H.F. Kung, A.D. Joshi, D.M. Skovronsky and M.J. Pontecorvo, *J. Nucl. Med.*, **51**, 913 (2010); https://doi.org/10.2967/jnumed.109.069088.
12. S.R. Choi, G. Golding, Z. Zhuang, W. Zhang, N. Lim, F. Hefti, T.E. Benedum, M.R. Kilbourn, D. Skovronsky and H.F. Kung, *J. Nucl. Med.*, **50**, 1887 (2009); https://doi.org/10.2967/jnumed.109.065284.
13. G.W. Small, V. Kepe, L. Ercoli, P. Siddarth, S.Y. Bookheimer, K.J. Miller, H. Lavretsky, A.C. Burggren, G.M. Cole, H.V. Vinters, P.M. Thompson, S.C. Huang, N. Satyamurthy, M.E. Phelps and J.R.N. Barrio, *Engl. J. Med.*, **355**, 2652 (2006); https://doi.org/10.1056/NEJMoa054625.

14. S.M. Ametamey, M. Honer and P.A. Schubiger, *Chem. Rev.*, **108**, 1501 (2008); https://doi.org/10.1021/cr0782426.
15. P.W. Thompson, L. Ye, J.L. Morgenstern, L. Sue, T.G. Beach, D.J. Judd, N.J. Shipley, V. Libri and A. Lockhart, *J. Neurochem.*, **109**, 623 (2009); https://doi.org/10.1111/j.1471-4159.2009.05996.x.
16. C.C. Rowe, U. Ackerman, W. Browne, R. Mulligan, K.L. Pike, G. O'Keefe, H. Tochon-Danguy, G. Chan, S.U. Berlangieri, G. Jones, K.L. Dickinson-Rowe, H.P. Kung, W. Zhang, M.P. Kung, D. Skovronsky, T. Dyrks, G. Holl, S. Krause, M. Friebe, L. Lehman, S. Lindemann, L.M. Dinkelborg, C.L. Masters and V.L. Villemagne, *Lancet Neurol.*, **7**, 129 (2008); https://doi.org/10.1016/S1474-4422(08)70001-2.
17. W. Zhang, S. Oya, M.-P. Kung, C. Hou, D.L. Maier and H.F. Kung, *Nucl. Med. Biol.*, **32**, 799 (2005); https://doi.org/10.1016/j.nucmedbio.2005.06.001.
18. W. Zhang, M.P. Kung, S. Oya, C. Hou and H.F. Kung, *Nucl. Med. Biol.*, **34**, 89 (2007); https://doi.org/10.1016/j.nucmedbio.2006.10.003.
19. R. Vandenberghe, K. Van Laere, A. Ivanoiu, E. Salmon, C. Bastin, E. Triau, S. Hasselbalch, I. Law, A. Andersen, A. Korner, L. Minthon, G. Garraux, N. Nelissen, G. Bormans, C. Buckley, R. Owenius, L. Thurfjell, G. Farrar and D.J. Brooks, *Ann. Neurol.*, **68**, 319 (2010); https://doi.org/10.1002/ana.22068.
20. S.T. Harrison, J. Mulhearn, S.E. Wolkenberg, P.J. Miller, S.S. O'Malley, Z. Zeng, D.L. Williams Jr., E.D. Hostetler, S. Sanabria-Bohorquez, L. Gammage, H. Fan, C. Sur, J.C. Culberson, R.J. Hargreaves, J.J. Cook, G.D. Hartman and J.C. Barrow, *ACS Med. Chem. Lett.*, **2**, 498 (2011); https://doi.org/10.1021/ml200018n.
21. A.B. Newberg, N.A. Wintering, K. Plossl, J. Hochold, M.G. Stabin, M. Watson, D. Skovronsky, C.M. Clark, M.P. Kung and H.F. Kung, *J. Nucl. Med.*, **47**, 748 (2006).
22. Z.P. Zhuang, M.P. Kung, A. Wilson, C.W. Lee, K. Plossl, C. Hou, D.M. Holtzman and H.F. Kung, *J. Med. Chem.*, **46**, 237 (2003); https://doi.org/10.1021/jm020351j.
23. M.P. Kung, C. Hou, Z.P. Zhuang, B. Zhang, D. Skovronsky, J.Q. Trojanowski, V.M. Lee and H.F. Kung, *Brain Res.*, **956**, 202 (2002); https://doi.org/10.1016/S0006-8993(02)03436-4.
24. L. Cai, F.T. Chin, V.W. Pike, H. Toyama, J.-S. Liow, S.S. Zoghbi, K. Modell, E. Briard, H.U. Shetty, K. Sinclair, S. Donohue, D. Tipre, M.-P. Kung, C. Dagostin, D.A. Widdowson, M. Green, W. Gao, M.M. Herman, M. Ichise and R.B. Innis, *J. Med. Chem.*, **47**, 2208 (2004); https://doi.org/10.1021/jm030477w.
25. G. Kuang, N.A. Murugan, Y. Tu, A. Nordberg and H. Ågren, *J. Phys. Chem. B*, **119**, 11560 (2015); https://doi.org/10.1021/acs.jpcb.5b05964.
26. (a) Z.P. Zhuang, M.P. Kung, C. Hou, D.M. Skovronsky, T.L. Gur, K. Plossl, J.Q. Trojanowski, V.M.Y. Lee and H.F. Kung, *J. Med. Chem.*, **44**, 1905 (2001); https://doi.org/10.1021/jm010045q.
(b) M. Ono, M. Ishikawa, H. Kimura, S. Hayashi, K. Matsumura, H. Watanabe, Y. Shimizu, Y. Cheng, M. Cui, H. Kawashima and H. Saji, *Bioorg. Med. Chem. Lett.*, **20**, 3885 (2010); https://doi.org/10.1016/j.bmcl.2010.05.027.
27. A.F. Martins, J.-F. Morn, A. Kubícková, V. Kubícek, F. Buron, F. Suzenet, M. Salerno, A.N. Lazar, C. Duyckaerts, N. Arlicot, D. Guilloteau, C.F.G.C. Geraldes and É. Tóth, *ACS Med. Chem. Lett.*, **4**, 436 (2013); https://doi.org/10.1021/ml400042w.
28. K. Serdons, K. Van Laere, P. Janssen, H.F. Kung, G. Bormans and A. Verbruggen, *J. Med. Chem.*, **52**, 7090 (2009); https://doi.org/10.1021/jm900871v.
29. M. Laruelle, M. Slifstein and Y. Huang, *Mol. Imaging Biol.*, **5**, 363 (2003); https://doi.org/10.1016/j.mibio.2003.09.009.
30. A.K. Tiwari, J. Yui, M. Fujinaga, K. Kumata, Y. Shimoda, T. Yamasaki, L. Xie, A. Hatori, J. Maeda, N. Nengaki and M.R. Zhang, *J. Neurochem.*, **129**, 712 (2014); https://doi.org/10.1111/jnc.12670.
31. K. Matsumura, M. Ono, H. Kimura, M. Ueda, Y. Nakamoto, K. Togashi, Y. Okamoto, M. Ihara, R. Takahashi and H. Saji, *ACS Med. Chem. Lett.*, **3**, 58 (2012); https://doi.org/10.1021/ml200230e.